Estimating the Hemispherical Broadband Longwave Emissivity of Global Vegetated Surfaces Using a Radiative Transfer Model

Article *in* IEEE Transactions on Geoscience and Remote Sensing · December 2015

DOI: 10.1109/TGRS.2015.2469535.

CITATIONS
36

READS
489

5 authors, including:

Jie Cheng
Beijing Normal University
128 PUBLICATIONS **3,359** CITATIONS

SEE PROFILE

Wout Verhoef
University of Twente
181 PUBLICATIONS **11,773** CITATIONS

SEE PROFILE

Qiang Liu
Beijing Normal University
183 PUBLICATIONS **3,474** CITATIONS

SEE PROFILE

Estimating the Hemispherical Broadband Longwave Emissivity of Global Vegetated Surfaces Using a Radiative Transfer Model

Jie Cheng, *Member, IEEE*, Shunlin Liang, *Fellow, IEEE*, Wout Verhoef, Linpeng Shi, and Qiang Liu

***Abstract*—Current satellite broadband emissivity (BBE) products do not correctly characterize the seasonal variation of vegetation abundance. This paper proposes a new method to estimate the BBE of vegetated surfaces to better describe the seasonal variation of vegetation abundance. The method takes advantage of the radiative transfer models' ability to calculate multiple scattering with a physical basis and uses the 4SAIL model to construct a lookup table (LUT) of BBE for vegetated surfaces. The BBE of the vegetated surface was derived from the LUT using three inputs: leaf BBE, soil BBE, and leaf area index (LAI). The validation results show that the accuracy of the new method exceeds 0.005 over fully vegetated surfaces. As a case study, this method was applied to data from 2003 to generate global vegetated surface BBE products for that year. An analysis of the results indicated that the derived BBE can correctly reflect seasonal variations in vegetation abundance that the data converted from the Advanced Spaceborne Thermal Emission and Reflection Radiometer (ASTER) and MODIS spectral emissivity products have been unable to reveal. The new method was also compared to the vegetation cover method (VCM). The VCM can correctly characterize seasonal variations in vegetation abundance. However, the classification of bare soil and vegetation in the VCM may produce step discontinuity in the calculated BBE. The new method is being implemented to produce a new version of the Global LAnd Surface Satellite (GLASS) BBE product over vegetated surfaces.**

***Index Terms*—Broadband emissivity (BBE), leaf area index (LAI), normalized difference vegetation index (NDVI), radiative transfer, remote sensing, surface radiation budget.**

Manuscript received November 28, 2014; revised February 16, 2015, July 14, 2015, and August 5, 2015; accepted August 11, 2015. Date of publication October 26, 2015; date of current version January 19, 2016. This work was supported in part by the National Natural Science Foundation of China under Grant 41371323 and Grant 41331173, by the National High Technology Research and Development Program of China under Grant 2013AA122801, by the Beijing Higher Education Young Elite Teacher Project under Grant YETP0233, and by the International S&T Cooperation Program of China under Grant 2012DFG21710.

J. Cheng and L. Shi are with the State Key Laboratory of Remote Sensing Science, School of Geography, Beijing Normal University, Beijing 100875, China (e-mail: brucechan2003@126.com).

S. Liang is with the State Key Laboratory of Remote Sensing Science, School of Geography, Beijing Normal University, Beijing 100875, China, and also with the Department of Geographical Science, University of Maryland, College Park, MD 20742 USA.

W. Verhoef is with the Faculty of Geo-Information Science and Earth Observation (ITC), University of Twente, 7514 AE Enschede, The Netherlands.

Q. Liu is with the College of Global Change and Earth System Science, Beijing Normal University, Beijing 100875, China.

Color versions of one or more of the figures in this paper are available online at http://ieeexplore.ieee.org.

Digital Object Identifier 10.1109/TGRS.2015.2469535

I. Introduction

LAND surface emissivity (LSE) is an intrinsic property of the earth's surface determined by its composition and physical state, and it can be used for terrestrial and planetary geological studies, bedrock mapping, and resource exploration [1]–[8]. LSE can also be used as input data for land surface temperature (LST) retrieval algorithms [9]–[11]. Broadband emissivity (BBE, 4–100 μm) is an essential parameter in the estimation of surface upward longwave radiation, which is one of the four components in the land surface radiation budget. It is defined by net radiation and is a critical component of any land surface model characterizing hydrological, ecological, and biogeochemical processes [12]–[19]. Due to the lack of reliable observations, a constant emissivity value or very simple parameterizations are currently used in land surface models [20]–[22]. Previous studies indicate that more realistic satellite-derived BBE values could improve the simulation results of climate models [21], [22]. In addition, finer spatial resolution and higher temporal resolution of such data would be useful for surface energy balance studies at the local scale and serve as medium scales for the validation of coarse-resolution data, thereby improving our understanding of land–atmosphere interactions [14], [23], [24].

Three types of methods can be used to produce land surface BBE at the regional and global scales. The first method is the classification-based method. In this method, each land surface type is assigned a constant BBE value derived from laboratory-measured emissivity data. For example, Wilber *et al.* divided the earth's surface into a $10' \times 10'$ spatial resolution grid, categorized the land surface into 18 scene types, and generated a global BBE (5–100 μm) map by assigning a constant BBE value to each type based on the laboratory-measured spectral data [25]. The vegetation cover method (VCM) [26] and normalized difference vegetation index (NDVI) threshold method [11] are widely used to predetermine surface emissivity for the purpose of retrieving LSTs. Both methods classify the land surface as vegetated and nonvegetated, and they use static emissivity values for each component (soil and vegetation). These values are introduced into a physical model that defines the effective emissivity of the surface, in terms of an estimated vegetation fraction dynamically obtained from NDVI. These methods are also considered classification-based methods.

The second method involves converting existing narrowband emissivity to BBE. The BBE within a certain window (e.g., the 8–13.5-μm spectral range) can be expressed as a linear

combination of Advanced Spaceborne Thermal Emission and Reflection Radiometer (ASTER) or Moderate Resolution Imaging Spectroradiometer (MODIS) narrowband emissivity data [24]. Using this method, Ogawa *et al.* mapped global monthly BBE (8–13.5 μm) using the MODIS emissivity product (approximately 5 km) and a North African BBE (8–13.5 μm) using the ASTER emissivity product (90 m) [24], [27].

The third method directly establishes the relationship between BBE and optical data [28], [29]. This method was initially designed to estimate global 1-km eight-day BBE over bare soil from the MODIS narrowband albedo product [28], after which it was expanded to estimate global 1-km eight-day BBE over vegetated surfaces from the MODIS narrowband albedo and NDVI products [30]. This method was further expanded to estimate global 0.05° eight-day land surface BBE from AVHRR visible and near-infrared (VNIR) data [31].

The BBE retrieval accuracy of the first method is relatively poor. Soil BBE derived by converting ASTER narrowband emissivity can vary from 0.86 to 0.98 [28]. If a common static value of 0.96 is used for soil BBE, errors can reach 0.1. The accuracy of classification-based methods could be improved, provided that more types of component emissivity are considered [32]. BBE products derived from the second method have not been validated [27]. In addition, typically the spatial or temporal resolutions of the derived BBE using these two methods are limited. For example, the spatial resolution of the BBE map produced by Wilber *et al.* is coarse, and ASTER's revisit period is 16 days. The third method has been used to produce a Global LAnd Surface Satellite (GLASS) BBE data set for the years from 1981 to 2010. The GLASS BBE achieves an accuracy of 0.02 for pseudoinvariant sites [33] and is superior to the BBE data sets converted from existing satellite emissivity products [34].

Usually, LSE increases with vegetation abundance, a fact that has been verified by both experimental and modeling studies [35], [36]. There is no doubt that the BBE should also depict such variation in vegetated surfaces, i.e., BBE should increase with vegetation abundance. According to a previous study, the seasonal variation of BBE derived from ASTER is incorrect, and the seasonal variation of BBE derived from the MODIS emissivity product is irrational at six surface radiation budget network (SURFRAD) sites; these inaccuracies were thought to be incurred from inaccurate raw emissivity data [37]. The corresponding vegetation indexes and soil moistures exhibit good seasonal variations; however, the ASTER BBE is abnormal, and the MODIS BBE remains unchanged during the entire growing season. The seasonal variation of the GLASS BBE was also irrational for vegetated surfaces [34].

According to the studies mentioned earlier, it is impractical to derive vegetated surface BBEs that reflect correct seasonal variations using the aforementioned BBE estimation methods. Therefore, the objective of this study is to explore a new method to estimate BBE over vegetated surfaces that correctly characterizes seasonal variations. The rest of this paper is arranged as follows: the data used in this study are described in Section II; the methodology is described in Section III; results and discussion are presented in Sections IV and V; and the conclusions are given in Section VI.

II. Data

A. Satellite Data

The GLASS BBE data [38], GLASS leaf area index (LAI) data [38], MODIS NDVI data MOD13A2 [39], and MODIS land cover data MCD12Q1 [40] were used to generate a new BBE product over vegetated surfaces.

Theoretically, the spectral domain needed to calculate surface longwave net radiation is the total longwave range, whereas existing thermal infrared (TIR) sensors can only provide several discrete narrowband emissivity values within the spectral range of 3–14 μm. Using simulated emissivity spectra for snow, water, and minerals at 1–200 μm, Cheng *et al.* were able to investigate the accuracy of surface longwave net radiation estimates using remotely sensed BBE in different spectral domains (e.g., 3–14, 8–12, 8–13.5, 3-∞, and 0-∞ μm), and they found that BBE at 8–13.5 μm is the most accurate [41]. Thus, the spectral range of 8–13.5 μm was adopted for the GLASS BBE. The GLASS BBE product was derived from AVHRR and MODIS optical data using newly developed algorithms [3], [30], [31]. GLASS BBE was composed of two parts: global eight-day 1-km land surface BBE retrieved from seven MODIS black-sky albedos ranging from 2000 to 2010, and the global eight-day 0.05° land surface BBE retrieved from the AVHRR VNIR reflectance from 1981 to 1999. The BBE derived from the MODIS albedos was validated using field measurements conducted over desert areas in the United States and China, and the absolute difference was found to be 0.02 [28], [33].

The GLASS LAI product was generated using a general regression neural network (GRNN) from the MODIS reflectance data [42]. The GLASS LAI product has spatial and temporal resolutions of 1 km and eight days, respectively, and is available from 1981 to 2012 [38]. The GLASS LAI product is spatially complete, and no gaps are present, even when the MODIS/AVHRR surface reflectance was contaminated due to clouds or missing data resulting from sensor failure [29]. Both GLASS BBE and LAI products are released by the Center for Global Change Data Processing and Analysis of Beijing Normal University. The temporal and spatial resolutions of the MODIS NDVI were 16 days and 1 km, respectively.

MCD12Q1 is a yearly land cover data set with a 500-m spatial resolution. The International Geosphere-Biosphere Program (IGBP) land cover classification distinguishes 17 different classes and was adopted from among several land cover classification systems. All of the satellite products used in this study have a sinusoidal projection, which is convenient for spatial matching.

The GLASS BBE was used to calculate the multiyear average for different soil types in this study. The MOD13A2 was used to identify vegetated surfaces. The MCD12Q1 was used to determine vegetation types based on which leaf BBE was determined. The GLASS LAI was used as an input for the 4SAIL radiative transfer model in the following section. To investigate the seasonal variation of BBE derived from different emissivity products, the GLASS BBE product, the ASTER emissivity product (AST05) estimated using the temperature and emissivity separation (TES) algorithm [1] and ground reflectance product (AST07) obtained from land-leaving radiances

corrected for solar irradiance [43], and the MODIS emissivity product (MOD11C2) were also included. MOD11C2 is an eight-day Level 3 global 0.05° latitude/longitude climate modeling grid product composited from the MODIS day/night algorithm-derived LST and LSE [44].

In addition, a soil taxonomy based on a reclassification of the 1994 Food and Agriculture Organization and United Nations Educational, Scientific and Cultural Organization soil map of the world combined with a soil climate map was used to determine the BBE of the soil background. There were 12 soil orders in the map. The map's spatial resolution was approximately 0.0333°, with 5400 × 10 800 pixels. The soil taxonomy was projected to a 1-km sinusoidal projection to match the GLASS and MODIS data used.

B. Field Measurements

Densely vegetation surfaces may serve as validation sites for TIR remote sensing because of their homogenous temperature and emissivity values [45]. The field-measured emissivity collected at the Valencia test site was used to validate the estimated BBE in this study. The Valencia test site is located in a large extension of rice crops south of Valencia, Spain. Rice crops are flood irrigated and show nearly full vegetation cover in July and August. The Valencia test site exhibited homogeneous temperature and emissivity values at different spatial scales [46], [47]. The measurement site was centered at 39°15′01″ N, 0°17′43″ W in 2004 and 39°15′54″ N, 0°18′28″ W in 2005. The radiometric signal was measured using CIMEL 312 four-channel radiometers (channels 1–4 were set at 8–13 μm, 11.5–12.5 μm, 10.5–11.5 μm, and 8.2–9.2 μm, respectively) on August 3 and 12, 2004 and July 12, 2005. The emissivity of the rice canopy was derived using the box method [48]. For additional details about the field measurements, please refer to Coll *et al.* [45]. The emissivity of the rice canopy at channel 1 was 0.983 ± 0.003.

On May 9, 2015, we conducted a field experiment on the wheat crop of Hebi city, Henan province, China. The wheat crop was at the filling growth stage and showed nearly full vegetation cover. The distribution of experimental sites is shown in Fig. 1. The blue areas with low NDVI values indicate villages and towns. The NDVIs extracted from MOD13A2 for four experimental sites exceed 0.82. The height of the wheat crop was approximately 75 cm. An LAI of approximately 4 was measured using the destructive method at the monitoring sites of the Hebi National Agricultural Meteorology Experiment Station. Measurements were taken under overcast conditions. The ground-leaving radiation was measured using a CIMEL 312 four-channel radiometer. An infrared golden plate was used to measure the environmental radiation. The radiometer was placed above the wheat canopy and the infrared golden plate, at an elevation of 20–30 cm. The view zenith angle of the radiometer was 10°, which corresponds to a field view of approximately 17 cm in diameter, assuming an observation height of 1 m. Wheat canopy and infrared golden plate measurements were taken alternately. The radiometer had three narrowband channels, and the ASTER TES algorithm is not suitable for low-spectral-contrast targets. Thus, the normalized

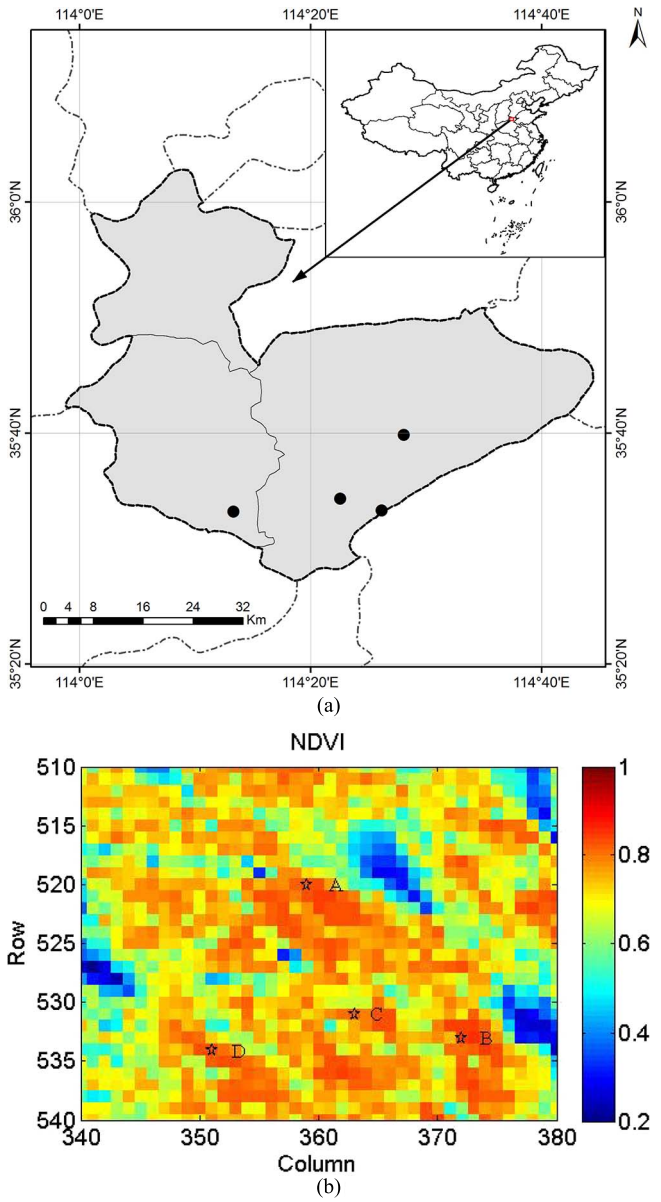

Fig. 1. Overview of the measurement sites. (a) Location of the sites in Hebi city, Henan province, China. (b) NDVI map extracted from MOD13A2 over the sites.

emissivity method (NEM) was used to determine the wheat canopy's emissivity [49], [50]. The NEM method-derived emissivity is relative emissivity, and its accuracy depends on the maximum emissivity value [51]. The maximum emissivities for the four-channel CIMEL 312 radiometer, as found in the ASTER spectral library, are 0.9908, 0.9780, and 0.9884, for conifers, deciduous, and grass, respectively [52]. The maximum emissivity of a field-measured and fully covered corn crop also approached 0.99 [53]. Thus, a maximum emissivity value of 0.99 was adopted. We collected three measurements of each variable at each site, and then, we randomly chose two points within a distance of ∼500 m from the site and collected three measurements for each variable at those points. The nine derived emissivity spectra were averaged to produce an emissivity value for the site. The measured emissivity for the wheat canopy is shown in Table I. The measured emissivity at

TABLE I
COMPARISON OF FIELD MEASURED EMISSIVITY AND RETRIEVED BBE

Site	Geolocation	Measured emissivity (Channel 1)	Retrieved BBE	
			1×1	3×3
A	(35.664° N, 114.468° E)	0.9828±0.0038	0.9878	0.9871±0.0017
B	(35.555° N, 114.436° E)	0.9845±0.0107	0.9879	0.9879±0.0001
C	(35.572° N, 114.376° E)	0.9859±0.0026	0.9879	0.9865±0.0016
D	(35.553° N, 114.222° E)	0.9820±0.0092	0.9851	0.9857±0.0019

channel 1 ranges from 0.9820 to 0.9859, which is very close to the measured emissivity of the rice crop in Spain.

III. METHODOLOGY

A. 4SAIL Model

To bridge the gap between the analytical canopy–soil models operating separately in the optical and TIR spectral domains, Verhoef *et al.* expanded the Scattering by Arbitrarily Inclined Leaves (SAIL) canopy reflectance model [54], [55] to include the TIR spectral domain and renamed it 4SAIL [56]. By adopting a safer and more robust formulation of the analytical solution, the 4SAIL model can overcome the numerical issues faced by its predecessors. The SAIL model family is based on a four-stream approximation of the radiative transfer equation, in which one distinguishes two direct fluxes (incident solar flux and radiance in the viewing direction) and two diffuse fluxes (upward and downward hemispherical fluxes). The interactions of these fluxes with the canopy are described by a system of four linear differential equations that can be solved. For the simplest case of a uniform vegetation temperature T_v, the model is based on the resolution of the following system of four linear equations:

$$\begin{aligned}
\frac{d}{Ldx}E_s &= kE_s \\
\frac{d}{Ldx}E^- &= -s'E_s + \alpha E^- - \sigma E^+ - \varepsilon_v H_v \\
\frac{d}{Ldx}E^+ &= sE_s + \sigma E^+ - \alpha E^+ + \varepsilon_v H_v \\
\frac{d}{Ldx}E_o &= \omega E_s + \nu E^- + \nu' E^+ - KE_o + K\varepsilon_v H_v
\end{aligned} \tag{1}$$

where E_s, E^-, E^+, and E_o are the direct solar irradiance on a horizontal plane, the diffuse downward irradiance, the diffuse upward irradiance, and the flux equivalent radiance in the direction of observation, respectively; L is the LAI; x is the relative optical height coordinate, which runs from -1 at the bottom of the canopy to 0 at the top; the coefficients k and K are the extinction coefficients for direct flux in the directions of the sun and the observer, respectively; s and s' are backscatter and forward scatter coefficients for specular flux, respectively; α is the attenuation coefficient; σ is the backscatter coefficient; ω is the bidirectional scatter coefficient for the downward view; ν and ν' are the directional backscatter and forward scatter coefficients for diffuse incidence, respectively; ε_v is the single-leaf emissivity; and the hemispherical flux H_v is the thermal emission of the blackbody leaves at temperature T_v. Note that, in principle, (1) applies to any monospectral radiation in the entire optical–thermal domain, although we realize that direct solar flux can generally be ignored in the TIR region, and TIR flux can be ignored in the solar-reflective regime. The analytical solution of (1) is given by

$$\begin{aligned}
E_s(-1) &= \tau_{ss}E_s(0) \\
E^-(-1) &= \tau_{sd}E_s(0) + \tau_{dd}E^-(0) + \rho_{dd}E^+(-1) + \gamma_d H_v \\
E^+(0) &= \rho_{sd}E_s(0) + \rho_{dd}E^-(0) + \tau_{dd}E^+(-1) + \gamma_d H_v \\
E_o(0) &= \rho_{so}E_s(0) + \rho_{do}E^-(0) + \tau_{do}E^+(-1) \\
&\quad + \tau_{oo}E_o(-1) + \gamma_o H_v
\end{aligned} \tag{2}$$

where the ρ values indicate the reflectances, and the τ values indicate the transmittances of the isolated canopy layer. The double subscripts indicate the types of flux on incidence and exit, respectively, where s stands for solar, d for diffuse hemispherical, and o for flux in the observer's direction. The various types of interaction [57] indicated by the double-subscript notation can be summarized by the following terms:

so bidirectional (reflectance);
ss direct (transmittance) in the direction of the solar beam;
sd directional–hemispherical (for solar flux);
dd bihemispherical;
do hemispherical–directional (in the viewing direction);
oo direct (transmittance) in the direction of observation.

Two new quantities, which are identified as the hemispherical and directional emissivity values of the isolated canopy layer, respectively, have been introduced and are given by

$$\begin{aligned}
\gamma_d &= 1 - \rho_{dd} - \tau_{dd} \\
\gamma_o &= 1 - \rho_{do} - \tau_{do} - \tau_{oo}.
\end{aligned} \tag{3}$$

For a Lambertian soil placed beneath the vegetation layer, one obtains the following equation:

$$E_o(-1) = E^+(-1) = r_s\left[E_s(-1) + E^-(-1)\right] + \varepsilon_s H_s \tag{4}$$

where r_s is the reflectance of the Lambertian soil, $\varepsilon_s = 1 - r_s$ is the soil emissivity, and H_s is the upward hemispherical thermal flux for soil temperature T_s. The unified solution for the entire optical–thermal spectral range can be derived by applying (2)–(4), as follows:

$$\begin{aligned}
E_o(0) &= \left[\rho_{so} + \frac{(\tau_{sd} + \tau_{ss})r_s(\tau_{do} + \tau_{oo})}{1 - r_s\rho_{dd}}\right]E_s(0) \\
&\quad + \left[\rho_{do} + \frac{(\tau_{do} + \tau_{oo})r_s\tau_{dd}}{1 - r_s\rho_{dd}}\right]E^-(0) \\
&\quad + \left[\gamma_o + \frac{(\tau_{do} + \tau_{oo})r_s\gamma_d}{1 - r_s\rho_{dd}}\right]H_v + \frac{(\tau_{do} + \tau_{oo})}{1 - r_s\rho_{dd}}\varepsilon_s H_v.
\end{aligned} \tag{5}$$

The directional emissivity of the soil–canopy system can be expressed as

$$\varepsilon_o = \gamma_o + \frac{(\tau_{do} + \tau_{oo})}{1 - r_s\rho_{dd}}r_s\gamma_d + \frac{(\tau_{do} + \tau_{oo})}{1 - r_s\rho_{dd}}\varepsilon_s. \tag{6}$$

The four-stream reflectance and transmittance quantities of the isolated canopy layer are all provided as regular output parameters of the 4SAIL model. The 4SAIL model can also incorporate four distinct component temperatures (sunlit soil temperature, shaded soil temperature, sunlit leaf temperature, and shaded leaf temperature), but this feature is not required for emissivity calculations [56]. The hemispherical emissivity was derived by integrating 4SAIL-modeled directional emissivity with the following equation [58]:

$$\varepsilon_H = 2\int_0^1 \varepsilon(\mu)\mu d\mu \tag{7}$$

where ε_H and $\varepsilon(\mu)$ are the hemispherical emissivity and 4SAIL-modeled directional emissivity using (6), respectively. μ is the cosine of the viewing zenith angle θ. Fig. 2 shows an example of 4SAIL-modeled hemispherical emissivity. When LAI values change from 0.1 to 6, which correspond to NDVI values from 0.189 to 0.946, the simulated hemisphere emissivity changes from 0.949 to 0.993. The hemispherical emissivity almost does not change when the LAI is greater than 3.

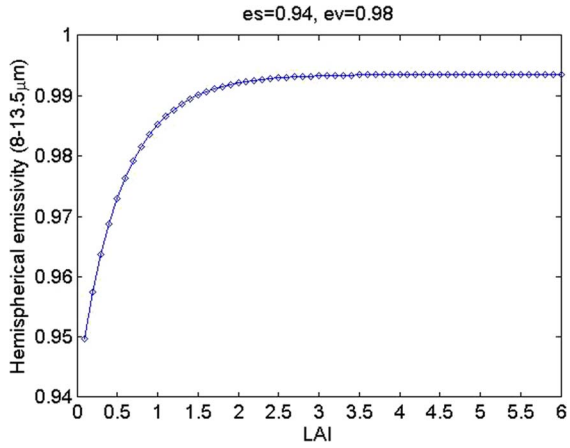

Fig. 2. Hemispherical emissivity derived from 4SAIL-simulated directional emissivity. Soil and leaf emissivity values were set at 0.94 and 0.98, respectively, and a spherical leaf inclination distribution function (LIDF) was used in the simulation.

B. Construction of the BBE LUT

The 4SAIL model was used to construct a BBE lookup table (LUT). To make the BBE LUT more flexible, the variation ranges for three principal model inputs were set as follows: The leaf BBE ranges from 0.935 to 0.995 and has an interval of 0.01; the soil BBE varies from 0.71 to 0.99 and has an interval of 0.01; and the LAI ranges from 0 to 6.0 and has an interval of 0.5. Vegetation canopy structures may vary greatly between species and cannot be easily assessed from ground measurements. Thus, a spherical distribution function has been widely used in environmental studies and radiative transfer models to denote this variable [36], [56], [59], [60]. According to Verhoef *et al.*, the difference between 4SAIL-modeled directional emissivity values using four LIDFs (planophile, plagiophile, spherical, and erectophile) are within 0.005, when the LAI ranges from 0.5 to 4 [56]. Therefore, a spherical distribution function was adopted. The spectral range was set to 8–13.5 μm in the simulation. We first used 4SAIL to model the directional BBE for view zenith angles ranging from 0° to 85° at 5° intervals. Then, the directional BBE was integrated to produce hemispherical BBE using (2). In total, there are 2710 situations represented in the constructed hemispherical BBE LUT.

TABLE II
LEAF BBE VALUES FOR SIX COMPOSITED VEGETATION LAND COVER TYPES

Composited Class	IGBP Class	BBE	Assignment of leaf emissivity
forest	1, 2, 3, 4, 5	0.9771	Mean of three live canopy BBEs from ASTER spectral library and 24 leaf BBEs from MODIS spectral library
grassland	10	0.9785	Mean of green grass BBE from ASTER spectral library and Pandya et al.[62]
cropland	12,14	0.9627	Mean of maize BBE, sorghum BBE, pearl millet BBE from Pandya et al[62], wheat BBE of Li et al. [63], and *Acer rubrum* BBE from Luz and Crowley[64]
savanna	8, 9	0.9778	50% Forest + 50% Grassland
shrubland	6, 7	0.9771	Forest
other types	16, 254	0.9785	Mean value of above five types

1–Evergreen Needleleaf Forest; 2–Evergreen Broadleaf Forest; 3–Deciduous Needleleaf Forest; 4–Deciduous Broadleaf Forest; 5–Mixed Forest; 6–Closed Shrublands; 7–Open Shrublands; 8–Woody Savannas; 9–Savannas; 10–Grasslands; 12–Croplands; 14–Cropland/Natural Vegetation; 16–Barren or sparsely vegetated; 254–Unclassified.

C. Determination of BBE Components

Only vegetated surfaces were considered in this study. The six vegetated land cover types in Table II were composited from 14 original IGBP land cover types. We have developed corresponding methods to determine BBE for bare soil, snow/ice, water, etc. Vegetated surfaces are assumed to be comprised of two primary components: vegetation canopy and soil background. Given the leaf and soil emissivities, as well as the structural parameters of a canopy, we can determine the emissivity spectra and BBE for a vegetated surface using a radiative transfer model. There are 24 laboratory-measured leaf emissivity spectra in the MODIS spectral library [61] and three live canopy emissivity spectra in the ASTER emissivity spectral library [52]. In addition, there are also a few field-measured leaf emissivity spectra in the literature. Table II gives the BBE values (8–13.5 μm) for six composited land cover types. Leaf emissivity was taken from the ASTER spectral library; the MODIS spectral library; and the measurements of Pandya *et al.* [62], Li *et al.* [63], and Luz and Crowley [64]. We averaged the emissivity spectra from different sources for composited IGBP forest, grassland, and cropland classes, and then, we calculated the corresponding BBE individually. Directionality was ignored in the calculation of BBE due to

a lack of directional emissivity measurements. The savanna vegetation type is mainly composed of herbaceous plants and woody plants; we averaged the BBEs of forest and grassland and classified the resulting value as the BBE for savanna. The prevailing vegetation type of shrubland is woody plants. Therefore, the BBE for shrubland was assigned the forest BBE value.

We calculated the mean BBE of each eight-day period for different soil types using the GLASS BBE from 2001 to 2010; the resulting value was designated the BBE of the soil background. The BBE for each soil type is shown in Fig. 3. The BBE variation in the Northern Hemisphere is different from that in the Southern Hemisphere. Spring and summer BBE values were larger than those for autumn and winter in the Northern Hemisphere, which may be consistent with the variation in soil moisture, assuming that the soil composition and surface microstructure do not change. In contrast, the BBE variation was minimal, and there were no significant variations, except those associated with the spodosol soil type, in the Southern Hemisphere.

D. BBE Estimation

Fig. 4 shows the flowchart outlining the process by which vegetated surface BBE values were estimated. The MODIS NDVI was used to identify a vegetated surface, according to the threshold 0.156, as defined in a previous study [65]. If the surface was vegetated, the MODIS yearly 500-m land cover product MCD12Q1 was used to determine the corresponding IGBP class, as described in Table II. A leaf BBE was assigned to each pixel based on the identified IGBP class. The leaf BBE of an aggregated 1-km pixel was obtained by averaging the leaf BBEs of four contiguous subpixels. The soil BBE was extracted, according to the soil type and satellite overpass time. The LAI was extracted from the GLASS LAI product. After determining these three inputs, the BBE of the vegetated surface was interpolated from the BBE LUT using leaf BBE, soil BBE, and LAI as indexes.

IV. Results

A. Direct Validation

We obtained the BBE of the Valencia test site for Julian days 209 and 225 in 2004. All retrieved BBE values for this site equaled 0.9878. The retrieved BBE of the 3×3 pixel array centered on each site also equaled 0.9878 ± 0.0001, which verified the homogeneity of the test site BBE data. The difference between the field-measured channel-1 emissivity and the retrieved BBE was 0.005. The spectral domain for the BBE was 8–13.5 μm, and the spectral domain mismatch between channel 1 (8–13 μm) and BBE was not considered.

The wheat crop BBE values for Julian day 129 in 2005 are presented in Table I. The standard deviation of the 3×3 pixel array centered on each site was less than 0.002, whereas the standard deviation of the measured emissivity for channel 1 occasionally reached 0.01. This may be attributed to the heterogeneity of the target incurred by the narrow field of view of the radiometer. However, in general, the experimental site can be considered homogeneous with relation to BBE. The maximum difference between measured emissivity and retrieved BBE is less than 0.005, and the mean difference is 0.003. The combined validation results of the two field experiments indicate that the accuracy of the retrieved BBE for nearly full vegetation cover surfaces is better than 0.005.

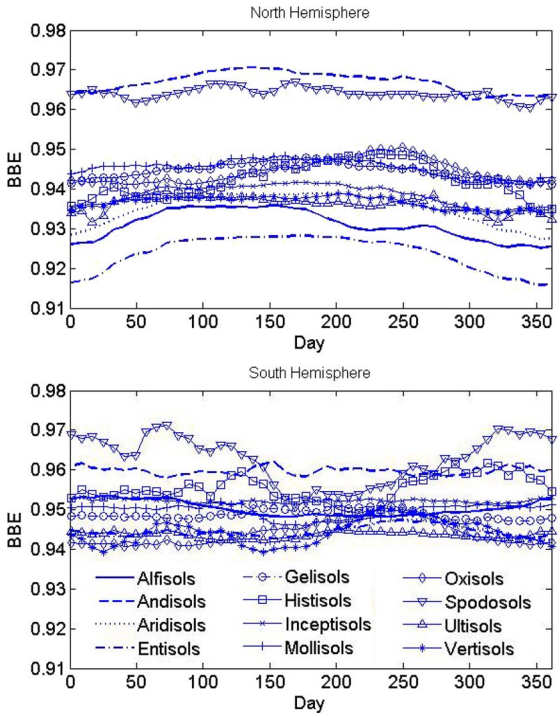

Fig. 3. Eight-day mean of GLASS BBE for each soil type. (Top) Northern Hemisphere. (Bottom) Southern Hemisphere.

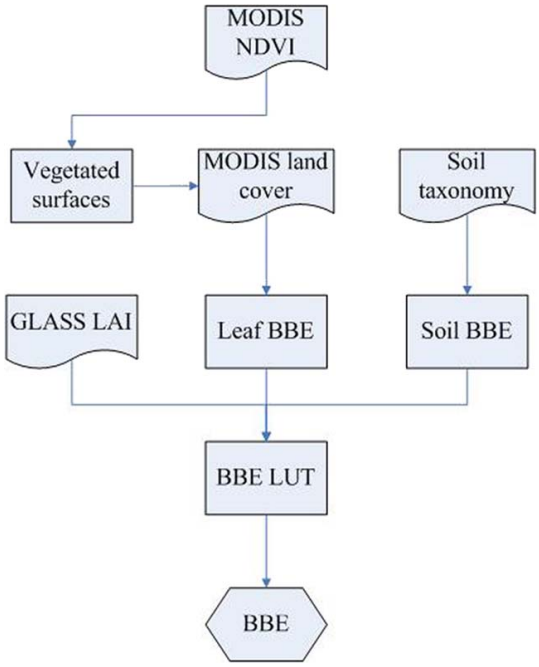

Fig. 4. Flowchart used to estimate BBE over vegetated surfaces.

B. Seasonal Variation

1) GLASS BBE Comparison: We used the aforementioned method to generate BBE for the year 2003. We randomly

selected pixels from relatively large areas with different dominant land cover types and analyzed the variations in their BBEs. Fig. 5 shows the estimated BBE for cropland, forest, grassland, savanna, and shrubland. The LAI was used as an indicator of vegetation abundance, as presented in Fig. 5. The GLASS BBE estimated using a previous algorithm [30] was also provided for comparison purposes. Note that BBE was set to 0.985, if the pixel was covered by snow or water. According to Table II and Fig. 3, almost all of the leaf BBE values are greater than the BBE values for soil background, with the exception of cropland. The BBE of vegetated surfaces should increase with increasing vegetation abundance. This behavior was fully characterized by the radiative transfer model (i.e., 4SAIL). As shown in Fig. 5, the seasonal variation of the newly derived BBE values agrees well with that of the LAI, for all vegetated land cover types, in the Northern and Southern Hemispheres. On the other hand, the seasonal variation of the GLASS BBE either has a negative correlation with LAI or is not significant. The incorrect seasonal variation observed in the GLASS BBE was generated by our previous algorithm, which estimates BBE using a linear combination of seven MODIS narrowband albedos and NDVI [34]. The variation in the GLASS BBE is mainly governed by the seasonal variation in the MODIS narrowband albedos. The seasonal variation of the narrowband albedo was either not significant or contrary to actual vegetation abundance. The variation in BBE magnitude was mainly controlled by the soil background BBE and the variation of the LAI; the variation of leaf BBE was not significant. For example, the variation in cropland BBE can reach 0.034 as the LAI changes from 0.3 to 4.1. At the start and end of the year, evergreen needleleaf forest (ENF) was covered by snow, and the variation of BBE was small, although the variation in the LAI was relative large. Grassland and shrubland BBE variation was less than 0.015 because the LAI variation was less than 0.2.

2) ASTER and MODIS Product Comparison: According to a previous study [34], the BBE calculated from the North American ASTER LSE Database (NAALSED) [66] for the summer season is lower than that calculated for the winter season. To further investigate the seasonal variation of the BBE calculated from the ASTER narrowband emissivity data, we selected test sites for each vegetated surface type from a relatively homogeneous area (the land cover remained unchanged from 2001 to 2010) using the MODIS yearly land cover type product MCD12C1. We downloaded the ASTER emissivity product AST05 and surface reflectance product AST07 for years from 2001 to 2010. The collection of ten years of ASTER data offsets the long revisit time and narrow swath of the ASTER data. The final BBE and NDVI were derived by averaging the BBE calculated from 11×11 ASTER pixels with Cheng *et al.*'s [41] formula and averaging the NDVI from 66×66 ASTER pixels. Representative results are shown in Fig. 6. Globally, the variation in the BBE contradicts the variation in NDVI for savanna, and the variation in the BBE resembles the variation in NDVI for cropland; however, the extreme values do not exactly match. It was difficult to identify a clear relationship between BBE and NDVI values for global deciduous broadleaf forest (DBF), ENF, and shrubland. These results indicate that we cannot derive accurate seasonal variations using BBE values derived from the ASTER emissivity data. We also investigated the seasonal variation in BBE, in 2003, calculated from the MODIS eight-day narrowband emissivity product MOD11C2 V5 for the same sites identified in Fig. 6. The corresponding new BBE and LAI are provided in Fig. 7, along with the results for the MODIS-based BBE. Clearly, there is no seasonal variation in the BBE derived from MOD11C2 V5, while the BBE derived in this paper fully characterized seasonal variations. We also investigated the seasonal variation in the BBE using the MOD11C2 V4 product and obtained similar results.

3) VCM Comparison: An alternative method to derive accurate seasonal variation may be the VCM, which is based on a model that defines the effective emissivity of a heterogeneous surface in relation to its structure, the vegetation cover percentage, and the thermal emissivity of its components [26], [67]. In this method, emissivity is expressed as

$$\varepsilon = \varepsilon_v P_v + \varepsilon_g (1 - P_v) + 4\langle d\varepsilon \rangle P_v (1 - P_v) \tag{8}$$

where ε_v is the vegetation emissivity, ε_g is the bare soil emissivity, and $\langle d\varepsilon \rangle$ is the cavity term related to the radiance emitted indirectly through internal reflections occurring between crop walls and the ground. A thorough analysis of the behavior of the cavity term was undertaken to consider a wide range of emissivity and structural conditions, and a formula was proposed to calculate the cavity term [67], as follows:

$$\begin{cases} \langle d\varepsilon \rangle = -0.435\varepsilon_g + 0.4343, & \varepsilon_v = 0.985 \\ \langle d\varepsilon \rangle = (-0.435\varepsilon_g + 0.4343)\left(\frac{\varepsilon_v}{0.985}\right), & \varepsilon_v \neq 0.985. \end{cases} \tag{9}$$

This relationship allows us to calculate the cavity term for any ground emissivity value. P_v is the fractional vegetation cover (FVC), which can be obtained from NDVI values using the following expression [68]:

$$P_v = \left(\frac{NDVI - NDVI_s}{NDVI_v - NDVI_s} \right)^2 \tag{10}$$

where $NDVI_v$ and $NDVI_s$ are the NDVI values of full vegetation cover and bare soil, respectively, which can be obtained from the NDVI histograms. In this paper, $NDVI_s$ and $NDVI_v$ were set equal to 0.156 and 0.461, respectively [65]. To obtain consistent values of P_v, the equation was set to zero for pixels with $NDVI < NDVI_s$ and one for pixels with $NDVI > NDVI_v$.

Taking cropland (35.55°, 114.22°) as an example, we compared the BBEs derived using the VCM and the method developed in this study. In the VCM, ε_v was assigned a field-measured value of 0.982, and ε_g was the same value as that used in the new method, i.e., the eight-day hemispherical mean of GLASS BBE for each soil type. The results are compared in Fig. 8. The BBE derived using each method correlate closely under fully vegetated surface conditions. Generally, the seasonal variation of the BBE derived using the VCM was consistent with that of the FVC. The difference in the two

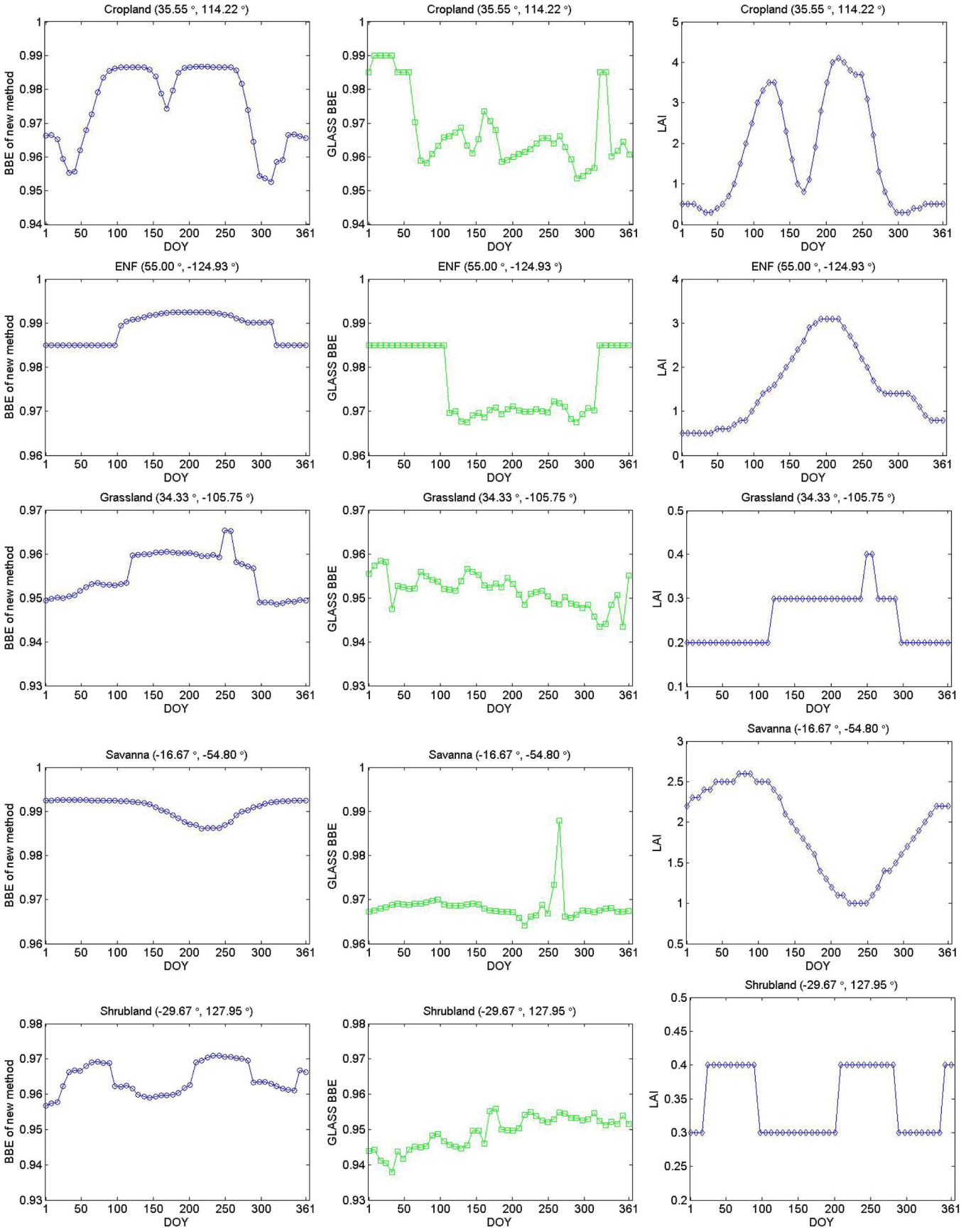

Fig. 5. New method for estimating BBE of cropland, forest, grassland, savannah, and shrubland (left) and its comparison with GLASS BBE (middle) estimations and the corresponding LAI (right).

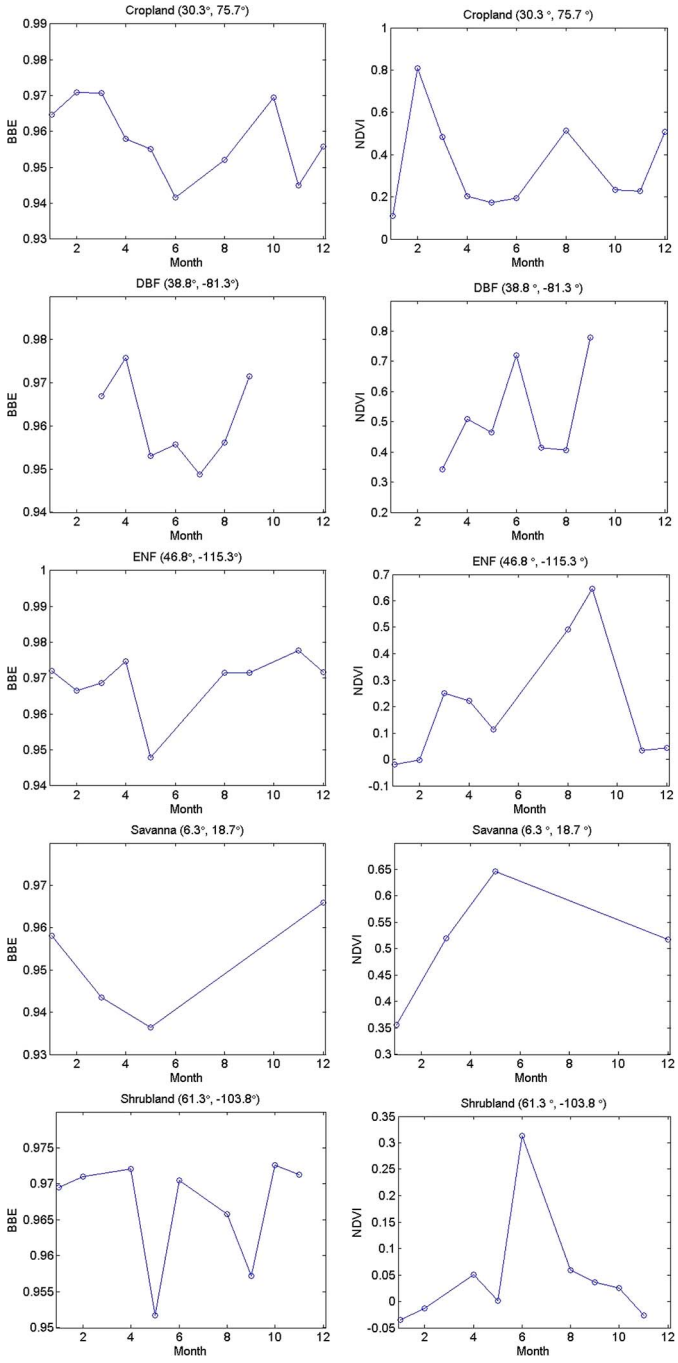

Fig. 6. Monthly averaged BBE derived from ASTER emissivity product AST05 for 2001–2010 compared to the matched NDVI values derived from ASTER surface reflectance product AST07.

methods' calculations of multiple scattering between leaves and the soil background may be the cause of the magnitude difference observed in the derived BBE. The classification of bare soil and vegetation produced step discontinuity in the calculated FVC and further caused step discontinuity in the calculated contribution of the cavity effect and the derived BBE in the VCM method. For example, the derived BBE on day 65 was greater than the BBE derived for day 81, which corresponds to full vegetation cover. Another drawback of the VCM is how difficult it is to determine the emissivity of the soil background at the global scale, which may change dramatically over the year, using this method.

V. Discussion

The magnitude of the BBE for nearly total vegetation cover derived in this paper was greater than that derived from the GLASS (see Fig. 5), that calculated from the ASTER emissivity data, and that calculated from the MODIS emissivity data (see Figs. 6 and 7). The main goal of the ASTER TES algorithm is to produce the spectral emissivity of soils and rocks, which guarantees its accuracy for soil and rocks. However, there are larger uncertainties when it is used to derive the emissivity for low spectral contrast surfaces such as vegetation, according to some experiments [69]. Our previous algorithm took the ASTER emissivity as a true value and established a linear relationship between the ASTER emissivity, MODIS spectral albedos, and NDVI. Thus, the GLASS BBE should be closer to the BBE calculated from the ASTER emissivity product and is likely to result in larger uncertainties over vegetated surfaces. The MODIS emissivity products derived using the day/night algorithm have not been extensively validated. Combined with the results of direct validation, the accuracy of the BBE derived over fully vegetated surfaces in this paper is superior to the GLASS BBE and that derived from the ASTER and MODIS emissivity data.

All of the aforementioned emissivity products are not well validated over partially vegetated surfaces due to a lack of ground-measured emissivity. Thus, it is difficult to determine their accuracy. Such data are highly valuable and desirable. Currently, it is technically difficult to measure the emissivity of vegetated surfaces from sparsely vegetated to nearly fully vegetated surfaces in the field. For a single measurement, it is difficult to determine the FVC in an instrument's field of view, as well as to determine the emissivity of the soil background. During an entire growth stage, it is difficult to maintain a consistent field of view for the length of time needed to obtain accurate measurements. According to the directional emissivity comparison results for canopies obtained by Sobrino *et al.* [36], the absolute emissivity difference between the analytical parameterization model based on the gap function (FRA^{RTM}) [59] and the volumetric model based on the BRDF estimation ($S\&W^{VM}$) [70] is less than 0.002; the absolute emissivity difference between the FRA^{RTM} and the 4SAIL radiative transfer model (VER^{RTM}) [56] is less than 0.0035; and the absolute emissivity difference between VER^{RTM} and $S\&W^{VM}$ is less than 0.005, all given a soil emissivity of 0.94 and a vegetation emissivity of 0.98. These values were obtained, when the LAI varied from 0.5 to 6 and the viewing angle varied from 0° to 70°. $S\&W^{VM}$ was used to determine the LSE for the MODIS split-window LST retrieval algorithm [61], [71]. The MODIS LST has been extensively validated and is well known for its high accuracy over homogeneous surfaces [72]–[74]. FRA^{RTM} and VER^{RTM} were applied to retrieve component temperatures from directional radiometric measurements and did so with acceptable accuracy [56], [75]. This suggests that these canopy emissivity models' simulated emissivity values and retrieved temperatures or component temperatures are self-consistent.

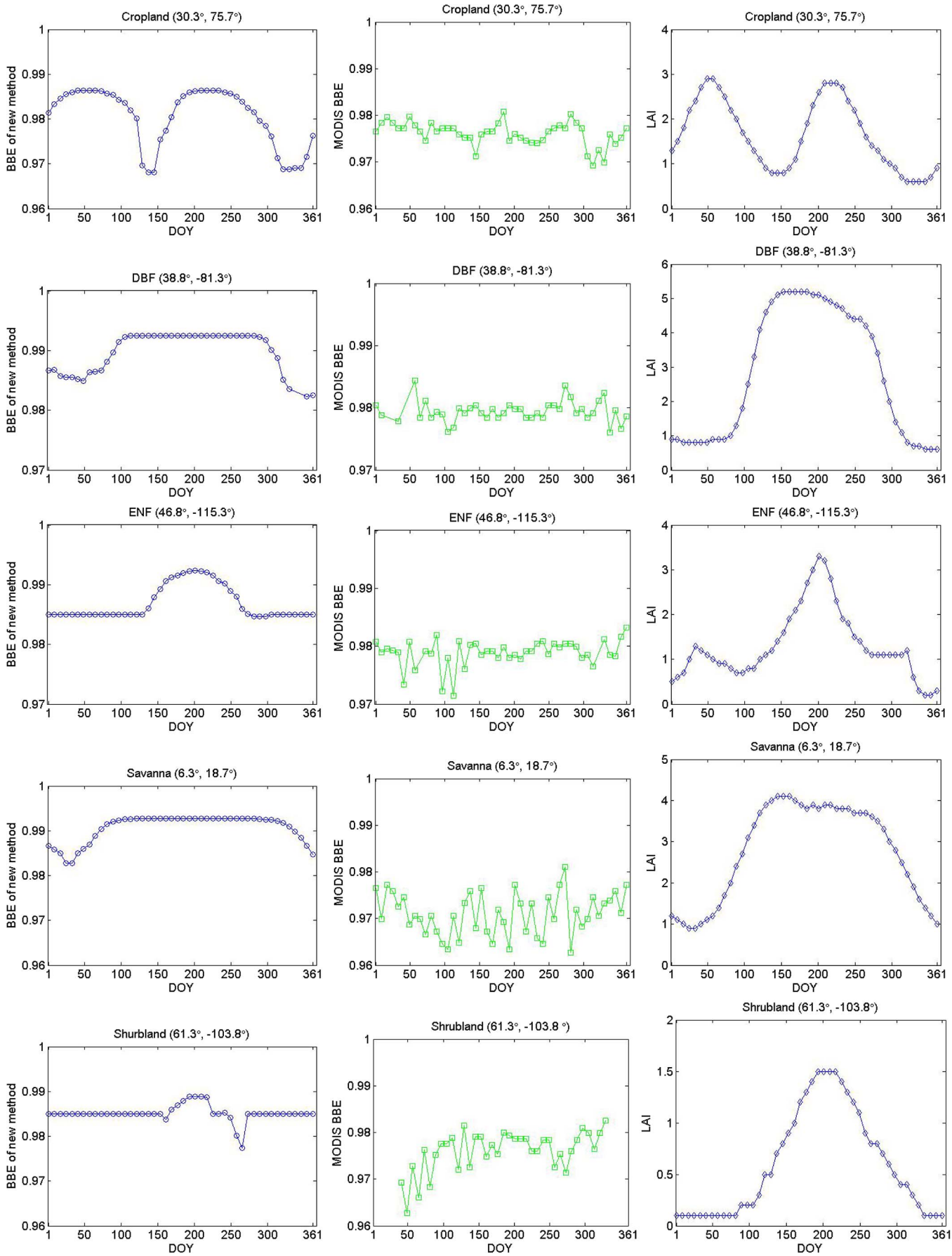

Fig. 7. (left) Comparison of the seasonal variation of new BBE, (middle) the BBE calculated from MODIS emissivity product MOD11C2, (right) and the corresponding LAI.

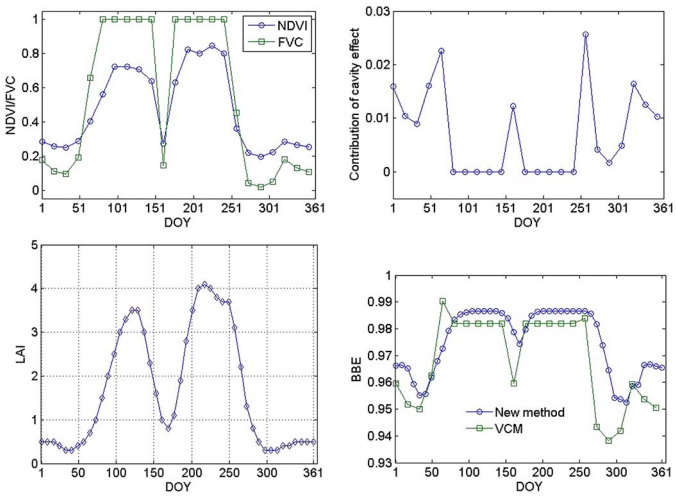

Fig. 8. Comparison of cropland BBE derived in this paper with that derived using the VCM (35.55°, 114.22°). The corresponding FVC, LAI, and the contribution of the cavity effect are also provided.

Therefore, the accuracy of the BBE derived over partially vegetated surfaces in this paper is acceptable.

There is an urgent need to carry out systematic ground measurements to obtain vegetated surface emissivity values for the entire growing season, to validate satellite emissivity data and radiative transfer models. However, this is beyond the scope of this paper.

The eight-day hemispherical mean of GLASS BBE for each soil type was used in the method developed in this paper. We will design a more practical method to incorporate simultaneously retrieved soil BBE into this method in the future.

VI. Conclusion

BBE is a key variable in the estimation of the surface radiation budget, which is the driving force of weather, climate, and environmental change. Previous studies have indicated that the BBEs calculated from the ASTER and MODIS emissivity products do not correctly characterize the seasonal variation of vegetation abundance, nor does the GLASS BBE product. Thus, we have proposed a new method to estimate BBE over vegetated surfaces to better reflect seasonal variations.

This new method is based on the LUT constructed using the radiative transfer model 4SAIL. The BBE of a vegetated surface can be derived from the LUT provided with the BBE of leaf, soil background, and LAI. To characterize the surface condition as accurately as possible, specific attention was paid to the input parameters. Each vegetated land cover type was assigned a leaf BBE by combining the MODIS land cover product with the leaf emissivities collected from the ASTER and MODIS spectral libraries and selected studies. Soil BBE was derived from the GLASS BBE product. A BBE value for each soil type at each eight-day interval in both the Northern and Southern Hemispheres was available. The LAI used was the GLASS LAI product, which is highly accurate and has good spatiotemporal continuity.

The new BBE was validated for a fully vegetated surface using the data collected from two field experiments. The accuracy was 0.005 over a rice crop and 0.003 over a wheat crop. We produced the BBE for a vegetated surface from the year 2003 and analyzed its seasonal variation. Compared with the GLASS BBE, the BBE derived using the new method agrees well with the LAI (an indicator of vegetation abundance), which means that the new BBE correctly describes the seasonal variation of vegetation abundance. We investigated the seasonal variation of the BBE derived from the ASTER and MODIS emissivity products. They failed to characterize the seasonal variation of vegetation abundance. We also compared the new method to the VCM. The seasonal variation of the BBE derived using the VCM was consistent with that of FVC. The classification of bare soil and vegetation in the VCM method may produce step discontinuity in the calculated BBE. Thus, the new method was selected to produce the next GLASS BBE product version for vegetated surfaces, which is scheduled to be released at the end of this year.

Acknowledgment

The ASTER and MODIS data were obtained from http://reverb.echo.nasa.gov/reverb/, the GLASS LAI was obtained from http://www.bnu-datacenter.com, and the soil taxonomy was obtained from http://soils.usda.gov/use/worldsoils/mapindex/order.html. The authors would also like to thank the anonymous reviewers for the valuable comments and suggestions that improve the presentation of this paper.

References

[1] A. R. Gillespie *et al.*, "A temperature and emissivity separation algorithm for Advanced Spaceborne Thermal Emission and Reflection Radiometer (ASTER) images," *IEEE Trans. Geosci. Remote Sens.*, vol. 36, no. 4, pp. 1113–1126, Jul. 1998.

[2] J. Cheng, S. Liang, Q. Liu, and X. Li, "Temperature and emissivity separation from ground-based MIR hyperspectral data," *IEEE Trans. Geosci. Remote Sens.*, vol. 49, no. 4, pp. 1473–1484, Apr. 2011.

[3] J. Cheng and H. Ren, "Land-surface temperature and thermal-infrared emissivity," in *Advanced Remote Sensing: Terrestrial Information Extraction and Applications*, S. Liang, X. Li, and J. Wang, Eds. New York, NY, USA: Academic, 2012, pp. 235–271.

[4] J. W. Salisbury and D. M. D'Aria, "Emissivity of terrestrial materials in the 8–14 [mu]m atmospheric window," *Remote Sens. Environ.*, vol. 42, pp. 83–106, 1992.

[5] A. N. French, T. J. Schmugge, and W. P. Kustas, "Discrimination of senescent vegetation using thermal emissivity contrast," *Remote Sens. Environ.*, vol. 74, no. 2, pp. 249–254, Nov. 2000.

[6] L. C. Rowan, J. C. Mars, and C. J. Simpson, "Lithologic mapping of the Mordor, NT, Australia ultramafic complex by suing the Advanced Spaceborne Thermal Emission and Reflection Radiometer (ASTER)," *Remote Sens. Environ.*, vol. 99, pp. 105–126, 2005.

[7] R. G. Vaughan, W. M. Calvin, and J. V. Taranik, "SEBASS hyperspectral thermal infrared data: Surface emissivity measurement and mineral mapping," *Remote Sens. Environ.*, vol. 85, no. 1, pp. 48–63, Apr. 2003.

[8] L. Kirkland *et al.*, "First use of airborne thermal infrared hyperspectral scanner for compositional mapping," *Remote Sens. Environ.*, vol. 80, no. 3, pp. 447–459, Jun. 2002.

[9] Z.-L. Li *et al.*, "Land surface emissivity retrieval from satellite data," *Int. J. Remote Sens.*, vol. 46, no. 2, pp. 1–44, Feb. 2013.

[10] S. Liang, "An optimization algorithm for separating land surface temperature and emissivity from multispectral thermal infrared imagery," *IEEE Trans. Geosci. Remote Sens.*, vol. 39, no. 2, pp. 264–274, Feb. 2001.

[11] J. A. Sobrino *et al.*, "Land surface emissivity retrieval from different VNIR and TIR sensors," *IEEE Trans. Geosci. Remote Sens.*, vol. 46, no. 2, pp. 316–327, Feb. 2008.

[12] P. J. Sellers *et al.*, "Modeling the exchange of energy, water and carbon between the continents and the atmosphere," *Science*, vol. 275, pp. 83–106, 1997.

[13] G. Bisht and R. L. Bras, "Estimation of net radiation from the MODIS data under all sky conditions: Southern Great Plains case study," *Remote Sens. Environ.*, vol. 114, no. 7, pp. 1522–1534, Jul. 2010.
[14] S. Liang, K. Wang, X. Zhang, and M. Wild, "Review of estimation of land surface radiation and energy budgets from ground measurements, remote sensing and model simulation," *IEEE J. Sel. Topics Earth Observ. Remote Sens.*, vol. 3, no. 3, pp. 225–240, Sep. 2010.
[15] F. Jacob *et al.*, "Comparison of land surface emissivity and radiometric temperature derived from MODIS and ASTER sensors," *Remote Sens. Environ.*, vol. 90, no. 2, pp. 137–152, Mar. 2004.
[16] E. Pequignot, A. Chedin, and N. A. Scott, "Infrared continental surface emissivity spectra retrieved from AIRS Hyperspectral sensor," *J. Appl. Meteorol. Climatol.*, vol. 47. no. 6, pp. 1619–1633, Jun. 2008.
[17] G. R. Diak, W. L. Bland, J. R. Mecikalski, and M. C. Anderson, "Satellite-based estimates of longwave radiation for agricultural applications," *Agricultural Forest Meteorol.*, vol. 103, no. 4, pp. 349–355, Jul. 2000.
[18] J. M. Norman *et al.*, "Remote sensing of surface energy fluxes at 10-m pixel resolutions," *Water Resources Res.*, vol. 39, no. 8, pp. 1–18, Aug. 2003.
[19] K. Nishida, R. R. Nemani, S. W. Running, and J. M. Glassy, "An operational remote sensing algorithm of land evaporation," *J. Geophys. Res.*, vol. 108, no. D9, pp. 1–14, 2003.
[20] G. B. Bonan *et al.*, "The land surface climatology of the community land model coupled to the NCAR community climate model," *J. Climate*, vol. 15, no. 22, pp. 3123–3149, Nov. 2002.
[21] M. Jin and S. Liang, "An improved land surface emissivity parameter for land surface models using global remote sensing observations," *J. Climate*, vol. 19, no. 12, pp. 2867–2881, Jun. 2006.
[22] L. Zhou *et al.*, "A sensitivity study of climate and energy balance simulations with use of satellite-based emissivity data over Northern Africa and the Arabian Peninsula," *J. Geophys. Res.*, vol. 108, no. D24, p. 4795, 2003.
[23] A. N. French *et al.*, "Surface energy fluxes with the advanced spaceborne thermal emission and reflection radiometer (ASTER) at the Iowa 2002 SMACEX site (USA)," *Remote Sens. Environ.*, vol. 99, no. 1/2, pp. 55–65, Nov. 2005.
[24] K. Ogawa and T. Schmugge, "Mapping surface broadband emissivity of the Sahara Desert using ASTER and MODIS data," *Earth Interactions*, vol. 8, no. 7, pp. 1–14, May 2004.
[25] A. C. Wilber, D. P. Kratz, and S. K. Gupta, "Surface emissivity maps for use in satellite retrievals of longwave radiation," Nat. Aeronaut. Space Admin. (NASA), Washington, DC, USA, NASA Tech. Publ., NASA/TP-1999-209362, 1999. [Online]. Available: http://techreports.larc.nasa.gov/1trs]
[26] E. Valor and V. Caselles, "Mapping land surface emissivity from NDVI: Application to European, African, and South American areas," *Remote Sens. Environ.*, vol. 57, no. 3, pp. 167–184, Sep. 1996.
[27] K. Ogawa, T. Schmugge, and S. Rokugawa, "Estimating broadband emissivity of arid regions and its seasonal variations using thermal infrared remote sensing," *IEEE Trans. Geosci. Remote Sens.*, vol. 46, no. 2, pp. 334–343, Feb. 2008.
[28] J. Cheng and S. Liang, "Estimating the broadband longwave emissivity of global bare soil from the MODIS shortwave albedo product," *J. Geophys. Res.-Atmos.*, vol. 119, no. 2, pp. 614–634, Jan. 2014.
[29] S. Liang *et al.*, *Global LAnd Surface Satellite (GLASS) Products: Algorithm, Validation and Analysis*. Berlin, Germany: Springer-Verlag, 2013.
[30] H. Ren, S. Liang, G. Yan, and J. Cheng, "Empirical algorithms to map global broadband emissivities over vegetated surfaces," *IEEE Trans. Geosci. Remote Sens.*, vol. 51, no. 5, pp. 2619–2631, May 2013.
[31] J. Cheng and S. Liang, "Estimating global land surface broadband thermal-infrared emissivity from the advanced very high resolution radiometer optical data," *Int. J. Digit. Earth*, vol. 6, pp. 34–49, 2013.
[32] E. Caselles, E. Valor, F. Abad, and V. Caselles, "Automatic classification-based generation of thermal infrared land surface emissivity maps using AATSR data over Europe," *Remote Sens. Environ.*, vol. 124, pp. 321–333, Sep. 2012.
[33] L. X. Dong, J. Y. Hu, S. H. Tang, and M. Min, "Field validation of GLASS land surface broadband emissivity database using pseudo-invariant sand dunes sites in northern China," *Int. J. Digit. Earth*, vol. 119, no. 2, pp. 614–634, Jan. 2014.
[34] J. Cheng and S. Liang, "A comparative study of three land surface broadband emissivity datasets from satellite data," *Remote Sens.*, vol. 6, no. 1, pp. 111–134, 2014.
[35] A. Olioso, G. Soria, J. A. Sobrino, and B. Duchemin, "Evidence of low land surface thermal infrared emissivity in the presence of dry vegetation," *IEEE Geosci. Remote Sens. Lett.*, vol. 4, no. 1, pp. 112–116, Jan. 2007.
[36] J. A. Sobrino, J. C. Jimenez-Munoz, and W. Verhoef, "Canopy directional emissivity: Comparison between models," *Remote Sens. Environ.*, vol. 99, no. 3, pp. 304–314, Nov. 2005.
[37] K. Wang and S. Liang, "Evaluation of ASTER and MODIS land surface temperature and emissivity products using long-term surface longwave radiation observations at SURFRAD sites," *Remote Sens. Environ.*, vol. 113, pp. 1556–1565, 2009.
[38] S. Liang *et al.*, "A long-term Global LAnd Surface Satellite (GLASS) data-set for environmental studies," *Int. J. Digit. Earth*, vol. 6, pp. 5–33, 2013.
[39] A. Huete *et al.*, "Overview of the radiometric and biophysical performance of the MODIS vegetation indices," *Remote Sens. Environ.*, vol. 83, pp. 1417–1434, 2002.
[40] M. A. Friedl *et al.*, "MODIS Collection 5 global land cover: Algorithm refinements and characterization of new datasets," *Remote Sens. Environ.*, vol. 28, pp. 337–374, 2010.
[41] J. Cheng, S. Liang, Y. Yao, and X. Zhang, "Estimating the optimal broadband emissivity spectral range for calculating surface longwave net radiation," *IEEE Geosci. Remote Sens. Lett.*, vol. 10, no. 2, pp. 401–405, Mar. 2013.
[42] Z. Xiao *et al.*, "Use of general regression neural networks for generating the GLASS leaf area index product from time-series MODIS surface reflectance," *IEEE Trans. Geosci. Remote Sens.*, vol. 52, no. 1, pp. 209–223, Jan. 2014.
[43] M. Abrams, "The advanced spaceborne thermal emission and reflection radiometer (ASTER): Data products for the high spatial resolution imager on NASA's Terra platform," *Int. J. Remote Sens.*, vol. 21, no. 5, pp. 847–859, 2000.
[44] Z. Wan and Z.-L. Li, "A physics-based algorithm for retrieving land-surface emissivity and temperature from EOS/MODIS data," *IEEE Trans. Geosci. Remote Sens.*, vol. 35, no. 4, pp. 980–996, Jul. 1997.
[45] C. Coll *et al.*, "Temperature and emissivity separation from ASTER data for low spectral contrast surfaces," *Remote Sens. Environ.*, vol. 110, no. 2, pp. 162–175, Sep. 2007.
[46] C. Coll *et al.*, "Ground measurements for the validation of land surface temperatures derived from AATSR and MODIS data," *Remote Sens. Environ.*, vol. 97, no. 3, pp. 288–300, Aug. 2005.
[47] C. Coll *et al.*, "Evaluation of split-window and dual-angle correction methods for land surface temperature retrieval from Envisat/AATSR data," *J. Geophys. Res.*, vol. 111, no. D12, Jun. 2006, Art. ID. D12105.
[48] E. Rubio, C. Caselles, C. Coll, E. Valor, and F. Sospedra, "Thermal-infrared emissivities of natural surfaces: Improvement on the experimental set-up and new measurements," *Int. J. Remote Sens.*, vol. 24, no. 24, pp. 5379–5390, 2003.
[49] A. R. Gillespie, "Lithologic mapping of silicate rocks using TIMS," in *Proc. TIMS Data Users' Workshop*, 1985, pp. 29–44.
[50] J. A. Sobrino, Z.-L. Li, G. Soria, and J. C. Jimenez, "Land surface temperature and emissivity retrieval from remote sensing data," *Recent Res. Develop. Geophys.*, vol. 4, pp. 21–44, 2002.
[51] Z. L. Li, F. Becker, M. P. Stoll, and Z. Wan, "Evaluation of six methods for extracting relative emissivity spectra from thermal infrared images," *Remote Sens. Environ.*, vol. 69, no. 3, pp. 197–214, Sep. 1999.
[52] A. M. Baldridge, S. J. Hook, C. I. Grove, and G. Rivera, "The ASTER spectral library version 2.0," *Remote Sens. Environ.*, vol. 113, no. 4, pp. 711–715, Apr. 2009.
[53] J. C. Jimenez-Munoz, J. A. Sobrino, A. Gillespie, D. Sabol, and W. T. Gustafson, "Improved land surface emissivities over agricultural areas using ASTER NDVI," *Remote Sens. Environ.*, vol. 103, no. 4, pp. 474–487, Aug. 2006.
[54] W. Verhoef, "Light scattering by leaf layers with application to canopy reflectance modeling: The SAIL model," *Remote Sens. Environ.*, vol. 16, no. 2, pp. 125–141, Oct. 1984.
[55] W. Verhoef, "Earth observation modeling based on layer scattering matrices," *Remote Sens. Environ.*, vol. 17, no. 2, pp. 165–178, Apr. 1985.
[56] W. Verhoef, L. Jia, Q. Xiao, and Z. Su, "Unified optical-thermal four-stream radiative transfer theory for homogeneous vegetation canopies," *IEEE Trans. Geosci. Remote Sens.*, vol. 45, no. 6, pp. 1808–1822, Jun. 2007.
[57] F. E. Nicodemus, "Reflectance nomenclature and directional reflectance and emissivity," *Appl. Opt.*, vol. 31, no. 6, pp. 7669–7683, Jun. 1970.
[58] B. Hapke, *Theory of Reflectance and Emittance Spectroscopy*. New York, NY, USA: Cambridge Univ. Press, 1993.

[59] C. Francois, C. Ottle, and L. Prevot, "Analytical parameterization of canopy directional emissivity and directional radiance in the thermal infrared. Application on the retrieval of soil and foliage temperatures using two directional measurements," *Int. J. Remote Sens.*, vol. 18, no. 12, pp. 2587–2621, 1997.
[60] J. Ross, *The Radiation Regime and Architecture of Plant Stands*. New York, NY, USA: Springer-Verlag, 1981.
[61] W. C. Snyder, Z. Wan, Z. Zhang, and Y.-Z. feng, "Classification-based emissivity for land surface temperature measurement from space," *Int. J. Remote Sens.*, vol. 19, no. 14, pp. 2753–2774, 1998.
[62] M. R. Pandya *et al.*, "Field measurements of plant emissivity spectra: An experimental study on remote sensing of vegetation in the thermal infrared region," *J. Indian Soc. Remote Sens.*, vol. 41, no. 4, pp. 787–796, Dec. 2013.
[63] H. Li, Q. H. Liu, Y. M. Du, J. X. Jiang, and H. X. Wang, "Evaluation of the NCEP and MODIS atmospheric products for single channel land surface temperature retrieval with ground measurements: A case study of HJ-1B IRS data," *IEEE J. Sel. Topics Appl. Earth Observ. Remote Sens.*, vol. 6, no. 3, pp. 1399–1408, Jun. 2013.
[64] B. R. Luz and K. Crowley, "Spectral reflectance and emissivity features of broad leaf plants: Prospects for remote sensing in the thermal infrared (8.0–14.0 μm)," *Remote Sens. Environ.*, vol. 109, no. 4, pp. 393–405, Aug. 2007.
[65] M. Momeni and M. R. Saradjian, "Evaluating NDVI-based emissivities of MODIS bands 31 and 32 using emissivities derived by Day/Night LST algorithm," *Remote Sens. Environ.*, vol. 106, no. 2, pp. 190–198, Jan. 2007.
[66] G. C. Hulley and S. J. Hook, "The North American ASTER Land Surface Emissivity Database (NAALSED) Version 2.0," *Remote Sens. Environ.*, vol. 113, no. 9, pp. 1967–1975, Sep. 2009.
[67] E. Valor and V. Caselles, "Validation of the vegetation cover method for land surface emissivity estimation," in *Recent Research Developments in Thermal Remote Sensing*, V. Caselles, E. Valor, and C. Coll, Eds. Kerala, India: Res. Signpost, 2005, pp. 1–20.
[68] T. N. Carlson and D. A. Ripley, "On the relationship between NDVI, fractional vegetation cover, and leaf area index," *Remote Sens. Environ.*, vol. 62, no. 3, pp. 241–252, Dec. 1997.
[69] A. R. Gillespie *et al.*, "Residual errors in ASTER temperature and emissivity products AST08 and AST05," *Remote Sens. Environ.*, vol. 115, no. 12, pp. 3681–3694, Dec. 2011.
[70] W. C. Snyder and Z. Wan, "BRDF models to predict spectral reflectance and emissivity in the thermal infrared," *IEEE Trans. Geosci. Remote Sens.*, vol. 36, no. 1, pp. 214–225, Jan. 1998.
[71] Z. Wan and J. Dozier, "A generalized split-window algorithm for retrieving land-surface temperature from space," *IEEE Trans. Geosci. Remote Sens.*, vol. 34, no. 4, pp. 892–905, Jul. 1996.
[72] Z. Wan, Y. L. Zhang, Q. C. Zhang, and Z.-L. Li, "Validation of the land surface temperature products retrieved from Terra Moderate Resolution Imaging Spectrometer data," *Remote Sens. Environ.*, vol. 83, pp. 163–180, 2002.
[73] Z. Wan, Y. Zhang, Q. C. Zhang, and Z.-L. Li, "Quality assessment and validation of the MODIS global land surface temperature," *Int. J. Remote Sens.*, vol. 25, no. 1, pp. 261–274, 2004.
[74] Z. Wan, "New refinements and validation of MODIS land-surface temperature/emissivity products," *Remote Sens. Environ.*, vol. 112, no. 1, pp. 59–74, Jan. 2008.
[75] C. Francois, "The potential of directional radiometric temperatures for monitoring soil and leaf temperature and soil moisture status," *Remote Sens. Environ.*, vol. 80, no. 1, pp. 122–133, Apr. 2002.

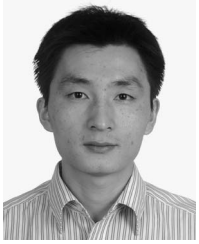

Jie Cheng (M'11) received the Ph.D. degree in cartography and remote sensing from the Institute of Remote Sensing Applications, Chinese Academy of Sciences, Beijing, China, in 2008.

He was a Postdoctoral Fellow with the State Key Laboratory of Remote Sensing Science, Beijing Normal University, from 2008 to 2010, and an Assistant Research Scientist with the University of Maryland, College Park, MD, USA, from 2009 to 2010. He is currently an Associate Professor with the State Key Laboratory of Remote Sensing Science, School of Geography, Beijing Normal University. His main research interests focus on estimation of land surface variables from satellite observations, radiative transfer modeling, and studies on surface energy balance.

Shunlin Liang (M'94–F'13) received the Ph.D. degree from Boston University, Boston, MA, USA.

He is currently a Professor with the School of Geography, Beijing Normal University, Beijing, China, and the Department of Geographical Sciences, University of Maryland, College Park, MD, USA. His main research interests focus on estimation of land surface variables from satellite data, Earth energy balance, and assessment of environmental changes. He has authored or coauthored over 220 SCI indexed journal papers, authored *Quantitative Remote Sensing of Land Surfaces* (Wiley, 2004), coauthored *Global LAnd Surface Satellite (GLASS) Products: Algorithms, Validation and Analysis* (Springer, 2013), edited *Advances in Land Remote Sensing: System, Modeling, Inversion and Application* (Springer, 2008), and coedited *Advanced Remote Sensing: Terrestrial Information Extraction and Applications* (Academic Press, 2012) and *Land Surface Observation, Modeling, Data Assimilation* (World Scientific, 2013).

Prof. Liang was an Associate Editor of the IEEE TRANSACTIONS ON GEOSCIENCE AND REMOTE SENSING and a Guest Editor of several remote-sensing-related journals.

Wout Verhoef was born in Sliedrecht, The Netherlands, in 1951. He received the Ing. degree in physics engineering in 1972 from the Technical College of Dordrecht, Dordrecht, The Netherlands, and the Ph.D. degree in agricultural and environmental sciences in 1998 from Wageningen University, Wageningen, The Netherlands, working on radiative transfer modeling in vegetation canopies and the atmosphere.

He started his career in optical remote sensing with the Netherlands Interdepartmental Working community for the Application of Remote Sensing techniques (NIWARS), Delft, The Netherlands, where he was involved in a field spectrometer measurement program on vegetation, soils, and water. In 1977, he joined the National Aerospace Laboratory (NLR), Amsterdam, The Netherlands, where he developed the widely known Scattering by Arbitrarily Inclined Leaves (SAIL) canopy reflectance model in 1981 and a range of improved variants. At NLR, he also developed image processing methodologies for time-series analysis (HANTS algorithm) and a wavelet-based data compression algorithm for hyperspectral images. He participated in several European Space Agency (ESA) studies, in preparation for a multiangular hyperspectral earth Explorer Mission. In 2005, he contributed in the ESA-China DRAGON Program with 12 lectures in Beijing, China. He was appointed as a Visiting Professor at the Beijing Capital Normal University. Since May 2006, he has been a Visiting Professor (30%) with the Faculty of Geo-Information Science and Earth Observation (ITC), Enschede, University of Twente, The Netherlands. He is a member of ESA's Fluorescence Explorer (FLEX) Mission Assessment Group.

Linpeng Shi received the B.S. and M.S. degrees in GIS from Beijing Normal University, Beijing, China, in 2012 and 2015, respectively.

He is currently with State Key Laboratory of Remote Sensing Science, School of Geography, Beijing Normal University. His current research interests include temperature and emissivity separation and multisource data integration.

Qiang Liu received the B.S. degree in computational mathematics from Peking University, Beijing, China, in 1997 and the Ph.D. degree in cartography and remote sensing from the Institute of Remote Sensing Applications, Chinese Academy of Sciences, Beijing, in 2002.

He is currently a Senior Scientist with the College of Global Change and Earth System Science, Beijing Normal University, Beijing, where he is also with the State Key Laboratory of Remote Sensing Science, which is jointly sponsored by the Institute of Remote Sensing Applications of Chinese Academy of Sciences and Beijing Normal University. His current research interests include multiangular remote sensing, such as geometric processing of multiangular images, BRDF/albedo modeling, and component temperature retrieval. His current research is to generate long time series of global BRDF/albedo from multiple remote sensing data sources.